TECHNICAL MEMORANDUM

Scaling of GNSS radio occultation impact with observation number using an ensemble of data assimilations

F. Harnisch, S. B. Healy, P. Bauer and S. J. English

Research Department

European Centre for Medium-Range Weather Forecasts
Europäisches Zentrum für mittelfristige Wettervorhersage
Centre européen pour les prévisions météorologiques à moyen terme

Abstract

An Ensemble of Data Assimilations (EDA) approach is used to estimate how the impact of Global Navigation Satellite System (GNSS) Radio Occultation (RO) measurements scales as a function of observation number in the ECMWF numerical weather prediction system. The EDA provides an estimate of the theoretical analysis and short-range forecast error statistics, based on the ensemble "spread", which is the standard deviation of the ensemble members about the ensemble mean. This study is based on computing how the ensemble spread of various parameters changes as a function of the number of simulated GNSS RO observations. The impact from 2000 up to 128000 globally distributed simulated GNSS RO profiles per day is investigated. It is shown that 2000 simulated GNSS RO measurements have a impact similar to real measurements in the EDA, and that the EDA based impact of real data can be related to the impact in observing system experiments. The dependence of the ensemble statistics on observation errors statistics assumed when assimilating the data, rather than the actual observation errors, is emphasized. There is no evidence of "saturation" of forecast impact even with 128000 GNSS RO profiles per day. However, this result is a well known consequence of always improving the theoretical analysis and short-range forecast error statistics when adding new observations that are assumed to have uncorrelated observation errors. In general, it is found that 16000 GNSS RO profiles per day have around half the impact of 128000 profiles, based on the reduction of ensemble spread values where the GNSS RO measurements have the largest impact.

1   Introduction

The Global Navigation Satellite System (GNSS) Radio Occultation (RO) measurement technique was demonstrated using Global Positioning System (GPS) signals in the GPS/-Meteorology (GPS/MET) (Kursinski et al., 1996; Rocken et al., 1997) and Challenging Minisatellite Payload (CHAMP) missions (Wickert et al., 2001). GNSS RO measurements from the Constellation Observing System for Meteorology, Ionosphere, and Climate (COSMIC) [1] satellites (Anthes et al., 2008), the GNSS Receiver for Atmospheric Sounding (GRAS) instrument on Metop-A (Luntama et al., 2008), and various missions of opportunity, such as GRACE-A (Wickert et al., 2009), TerraSAR-X (Beyerle et al., 2011), and C-NOFS, are now routinely assimilated at the operational numerical weather prediction (NWP) centers. They provide a total of around 2500 globally distributed profiles per day, and the GRAS instrument on Metop-B will add another 700 operational profiles from 2013.

Many NWP centers have reported a positive forecast impact with GNSS RO data (e.g., Healy and Thépaut 2006; Aparicio and Deblonde 2008; Poli et al. 2008; Rennie 2010; Cucurull 2010) despite the fact that GNSS RO data numbers are low when compared with the number of satellite radiances that are assimilated. For example, the European Centre for Medium-Range Weather Forecasts (ECMWF) assimilates around 10 million conventional and satellite observations per 12 hour period, of which 90 % are satellite radiance measurements, and only around 2-3 % are GNSS RO bending angles. The main GNSS RO impact is seen for upper-tropospheric and stratospheric temperatures. The GNSS RO measurements have a good impact because they provide complementary information to the satellite radiance measurements. Compared with satellite nadir sounders, the GNSS RO measurements have excellent vertical resolution, meaning they can detect signals (forecast errors) that are in the "null-space" (Rodgers, 2000) of the satellite radiance measurements. Further, GNSS RO measurements do not require bias correction, so they "anchor" the bias correction applied to satellite radiances (Auligné et al., 2007) and help identify NWP model biases.

It has been shown that GNSS RO measurements make a useful contribution to the Global Observing System (GOS) used for NWP. Furthermore, Observing System Experiments (OSEs) (Poli et al., 2008;

---

[1]also referred to as Formosat Satellite Mission (FORMOSAT-3) in Taiwan.

Bauer et al., 2013) indicate that the current GNSS RO observation number does not show any evidence of forecast impact "saturation", where any additional GNSS RO observations would introduce little extra benefit. Therefore, an important question in the context of designing – and trying to optimize – the future global observing system, is how the impact of GNSS RO observations scale if the data numbers are significantly increased, and to identify if this impact is likely to saturate. Estimating the impact of more measurements, and potentially predicting the point of observation impact saturation, requires the use of simulated GNSS RO measurements.

One approach is to perform Observing System Simulation Experiments (OSSEs) to test the impact of new data (Masutani et al., 2010). OSSEs are closely related to OSEs, but instead of analyzing the impact of real observations, OSSEs are based on simulating, and then subsequently assimilating, observations derived from a known "truth", represented by a "nature run", in order to estimate the forecast impact of the proposed observing system. OSSEs are computationally expensive because all observations have to be simulated. Recently, Tan et al. (2007) have proposed and developed an alternative approach to analyse the impact of simulated observations using the Ensemble of Data Assimilations (EDA) technique. They applied the EDA approach to estimate the impact of ESA's ADM-Aeolus wind profiling lidar. Unlike OSSEs, where all observations are simulated using an NWP forecast model to approximate the atmospheric state, in the EDA approach only the new observations are simulated. More specifically, the new observations are simulated from high quality NWP model fields, randomly perturbed in a manner which is consistent with the assumed observation error statistics, and then assimilated alongside real observations in the EDA. Tan et al. (2007) argue that this approach is superior to OSSEs, because the calculation is primarily based on real observations, with only the new data being simulated. However, we suggest that the EDA approach complements OSSEs, and that it is conceptually more closely related to a theoretical error covariance/information content study, similar to methods routinely used in one-dimensional satellite retrieval studies (Eyre, 1989, 1990). As with all EDA methods, the central assumption is that analysis and forecast error statistics (uncertainties) can be estimated from the "spread" of the ensemble members about the ensemble mean. If new observations are having a positive forecast impact, the spread of the ensemble of analyses and forecasts should be reduced. The relative impact of two observing systems can be determined by comparing to what extent they reduce the spread of the ensemble. This reduction is related to the impact of the new observing system.

In this study, we apply the EDA approach to estimate the impact of increasing the number of GNSS RO observations. A comprehensive set of simulated GNSS RO data is assimilated in a set of EDA experiments to assess the impact of the simulated GNSS RO profiles. The EDA analysis and forecast spread as a function of the GNSS RO observation number provides information on the impact of the observations, and how this impact scales with the observation number. The results are also compared with OSEs using real GNSS RO data.

Section 2 introduces the EDA approach, discusses the interpretation of the ensemble spread, and draws parallels with standard one-dimensional theoretical error covariance/information content studies. The simulation of GNSS RO bending angle profiles, the assimilation procedure and the performed EDA experiments are described in section 3. Results of the EDA experiments are covered in section 4, including a comparison of the observation impact based on the EDA approach and OSEs. The EDA spread results are discussed in section 5 and the main findings are summarized in section 6.

2 The Ensemble of Data Assimilations approach

The EDA is primarily designed to provide flow dependent analysis and short-range forecast error co-
variance information. An EDA has been used operationally at ECMWF since June 2010 (Isaksen et al.,
2010a; Bonavita et al., 2011), and it has had a significant positive impact on forecast scores (Bonavita
et al., 2012). In addition, the initial-time perturbations for the operational Ensemble System (ENS) are
constructed from the EDA estimate of analysis uncertainty (Buizza et al., 2010a). The theoretical jus-
tification of the EDA is given in Žagar et al. (2005) and Isaksen et al. (2010b), and the main points are
summarized in Appendix A.

If one accounts correctly for the different error sources in the NWP system, the analysis and forecast
error covariance matrices, $\mathbf{P}^a$ and $\mathbf{P}^f$, respectively, can be estimated from an ensemble of model analyses
and forecasts,

$$\mathbf{P}^a \simeq \mathbf{P}^a_e = \overline{(\mathbf{x}_a - \overline{\mathbf{x}}_a)(\mathbf{x}_a - \overline{\mathbf{x}}_a)^T} \tag{1}$$

$$\mathbf{P}^f \simeq \mathbf{P}^f_e = \overline{(\mathbf{x}_f - \overline{\mathbf{x}}_f)(\mathbf{x}_f - \overline{\mathbf{x}}_f)^T}. \tag{2}$$

The overbar denotes an expectation value, $\mathbf{x}_a$ ($\mathbf{x}_f$) is the model state vector at analysis (forecast) time and
$\overline{\mathbf{x}}$ represent the ensemble mean state vector.

The operational EDA at ECMWF – as of March 2013 – consists of a 10-member ensemble of 12-hourly
four-dimensional variational (4D-Var) data assimilation cycles that are run twice daily at 00 UTC and
12 UTC at a horizontal resolution of T399 wavenumber truncation. The EDA uses perturbed model
background fields, perturbed observations, perturbed sea surface fields, and perturbed model physics
to represent model error. The perturbations applied to the observations are uncorrelated and created
by a random draw from a Gaussian distribution with zero mean and standard deviation equal to the
estimate of the observation error standard deviation used in the assimilation (Isaksen et al., 2010b). For
atmospheric motion vector wind observations horizontally correlated perturbations are applied (Bormann
et al., 2003). Correlated patterns, as used in the ECMWF Seasonal Forecasting System (Vialard et al.,
2005), are used to perturb sea surface temperature fields. Model error is accounted for in both the
12-hourly 4D-Var data assimilation window and the longer range forecasts by stochastically perturbing
the total parametrized tendency of physical processes which is done with the Stochastically Perturbed
Parametrised Tendency (SPPT) scheme (Palmer et al., 2009). The same method is used to account for
model error operationally in the ENS (Buizza et al., 1999). The model background fields should not be
perturbed explicitly. A cycling EDA naturally provides an estimate of the model short-range forecast
uncertainty which is then used as model background information in the subsequent assimilation cycles
(See Fig. 2 of Tan et al. 2007). The first assimilation cycle, when the EDA is "cold started", has only
observations and model physics perturbed and model background fields are the same. The initialization
from identical model background fields leads to a spin-up time of the EDA, and after about one week the
ensemble of short-term forecasts represents the background error statistics of the NWP system (Fisher
et al., 2005). If observation and model perturbations have been drawn from the correct error covariances,
the spread of the EDA ensemble will represent the variance of analysis and short-range forecast errors of
the underlying NWP system correctly.

2.1 Properties of the EDA spread

Instead of considering the full analysis and forecast error covariance matrices, only the analysis and
forecast error variance estimated from the ensemble information is evaluated in this study. The EDA

spread is defined as

$$s = \sqrt{\mathbb{E}\left(\sigma_d^2\right)} = \sqrt{\frac{1}{D}\sum_{d=1}^{D}\left[\frac{1}{N-1}\sum_{n=1}^{N}\left(\mathbf{x}_n - \bar{\mathbf{x}}\right)^2\right]_d} \tag{3}$$

where $\mathbb{E}(.)$ denotes the expectation operator, $\mathbf{x}_n$ the model state for each single ensemble member and $\bar{\mathbf{x}}$ the ensemble mean model state. N is the size of the ensemble which is 10 here, and D specifies the period of interest.

The EDA spread values provide information about the theoretical forecast and analysis error statistics for the ECMWF NWP system, rather than information about any specific realization of these errors in a given forecast or analysis state. The spread values are determined by the assumed observation and model error statistics used to generate the perturbations applied in the EDA system, the observation operator used to assimilate the data, and the background error covariance matrix used in each ensemble member. The dependency of the EDA spread to the assumed observation error statistics, rather than the actual errors of the observations (or model analysis/forecast state), is key to interpreting many of the results presented in this study. It can be understood by noting that the estimated error statistics in a linear Kalman Filter are written in terms of the assumed input error covariances (Appendix A), and also by referring to the Ensemble Kalman Filter (EnKF, e.g., Burgers et al. 1998), which provides the theoretical framework for the EDA (Isaksen et al., 2010b). The computation of the error covariance matrices in the EnKF is separated from the update and forecast equations of the model state, and is a function of the respective input error covariances. The use of simulated observations is not expected to have an unrealistic effect on EDA spread values, because the assumed observation error covariance is the same for both simulated and real observations. This result is demonstrated in section 4.

It is known that the EDA spread itself is affected by errors which can be separated into random or sampling errors and systematic errors (Bonavita et al., 2011, 2012). Sampling errors arise from the small ensemble size (e.g., 10 members here) used for the spread computation. This type of error can be reduced by increasing the size of the ensemble, but it decreases only with the square root of the ensemble size. This slow rate of decrease of the random error means that for all current feasible number of ensemble members ($O(10\text{-}100)$), an objective filtering is required to reduce the sample noise in the EDA spread (Raynaud et al., 2009; Bonavita et al., 2011). A spectral low-pass filter has been applied successfully which enables the large scale signal of interest to be extracted while the small scale noise is filtered out (Bonavita et al., 2011). Systematic errors of the EDA spread result from an imperfect specification of the main errors sources which are assumed to be represented correctly in the EDA system. These errors can reflect the deficiencies in the specification of either the observation, background, and model error covariance matrices, respectively, or uncertainties in the boundary conditions which are not correctly accounted for. In the present EDA implementation there are still deficiencies in the applied perturbations which cause the ensemble to be underdispersive. To account for this, a calibration procedure enforcing statistical consistency between the EDA variance estimate and the ensemble mean error (Leutbecher, 2009) is applied operationally (Bonavita et al., 2012).

The EDA spread values used in this study are raw estimates which have not been corrected for random or systematic errors. By averaging the EDA spread on the hemispheric or global scale, the small scale noise to a large degree averages out, so it does not affect the large scale average of the EDA spread. In early studies with the EDA system (e.g., Isaksen et al. 2007; Tan et al. 2007), a constant global inflation factor close to 2 has been applied to the EDA spread to account for the systematic errors. However, more recent investigations have found that typically the systematic errors do not have a spatially homogeneous structure and the calibration factors are spatially and temporally varying (Bonavita et al., 2012). No calibration of the EDA spread is applied in this study as the varying calibration factors are likely to

influence also the observation impact. It is assumed that the systematic errors of the EDA spread are similar for all EDA experiments since they all use the same specification of the input error sources. Hence, it is not necessarily required to apply a constant calibration factor when the difference between EDA spread values, which determines the observation impact, is evaluated. Nevertheless, it needs to be considered that any quantitative values of the EDA spread are most likely too small since the ensemble is underdispersive.

With the EDA spread aiming to estimate the analysis and forecast error variance, the EDA approach essentially can be considered as a 4D-Var theoretical error covariance/-information content study. A number of analogous studies have been performed to derive the theoretical error statistics/information content of satellite observations in one-dimensional variational (1D-Var) retrievals of profile information. The 1D-Var calculations are based on assumed background and observation error statistics, and the observation operator used to assimilate the data. They have proven to be a valuable tool to investigate the potential impact of satellite observations and the optimal usage of the data by testing different retrievals, forward operators or channel selection strategies using the theoretical error characteristics of the solution error covariance matrix (e.g., Eyre (1990); Rabier et al. (2002)). These studies are often performed prior to the availability of the real data, but they are useful providing realistic assumptions are made about the error characteristics of the measurement. The 1D-Var problem is mathematically equivalent to the 4D-Var problem, but the dimensions of the covariance matrices in the 4D-Var case are far too large to be computed directly. The EDA provides an estimate of the theoretical analysis (forecast) error variance in the full 4D state of the atmosphere, including the impact of millions of observations and the forecast model, by using the ensemble spread.

3 Experimental setup

3.1 Simulation of GNSS RO data

Estimating the impact of GNSS RO measurements as a function of observation number requires to use simulated GNSS RO measurements because only 2000-3000 real GNSS RO profiles per day are available currently.

The generation of the simulated GNSS RO data is composed of three steps. At first, the time and location of the simulated observations has to be defined. It has been assumed that the observations are distributed randomly on the surface of a sphere. No "tangent point" drift has been included in the simulation process, so a single location is used for the entire profile of GNSS RO bending angle observations. The simulated profiles are temporally randomly distributed within 6-hourly time batches, centered on 0, 6, 12 and 18 UTC. No satellite orbit modeling has been applied here, but the random temporal and spatial distribution for the simulated GNSS RO data is expected to be a reasonable first-order approximation of the location and time of potential real profiles.

The operational ECMWF NWP analysis, computed with model version 33R1 at a horizontal resolution of T799 wavenumber truncation, acts as proxy for the truth and, in the second step, is interpolated to the previously derived observation location and time. Unlike Tan et al. (2007), where the observations were simulated from a short-term forecast of the Met Office model, we use ECMWF operational analyses to provide the model state for the simulation of the GNSS RO data. We note that these analyses are produced with an earlier ECMWF model cycle, and have a higher horizontal resolution than is used in the EDA experiments performed in this study. Nevertheless, using closely related NWP systems to first simulate data, and then assimilate it can be problematic in OSSEs, and possibly leads to over-optimistic

results. Tan et al. (2007) also suggest that it could lead to over-optimistic results in EDA based estimates. However, we do not believe this approach is problematic in the EDA, because the EDA spread values, which are used to estimate the theoretical error statistics and characterize the observation impact, are sensitive to the assumed input error statistics used to generate the perturbations added to the ensemble, rather than the actual errors of the observations or the model state (see section 2).

A two-dimensional (2D) bending angle operator (Healy et al., 2007) is applied to the operational ECMWF NWP analysis to generate profiles of ionosphere-corrected bending angles, α, as function of impact parameter, a. The impact parameter, a, defines the radius of closest approach the ray-path would have in the absence of bending. Mathematically, it is the product of the refractive index, n, the radius of the ray-path, r, and the sine of the angle, ϕ, between the local radius vector and the tangent to the ray path. Each simulated profile contains bending angles on the 247 fixed impact heights, h, (impact parameter, a, minus the radius of curvature, R_c) which are used for the operational GRAS measurements provided by the European Organisation for the Exploitation of Meteorological Satellites (EUMETSAT).

Finally, errors are added to the simulated GNSS RO bending angles before they can be used in NWP experiments. We have information about the departure statistics of real GNSS RO measurements which is useful for this step. The basic global error model is defined as 10 % of the observed value at $h = 0$, decreasing linearly to 1 % at $h = 10$ km, and 1 % above 10 km until this reaches a lower limit of 2 microradians. It is necessary to inflate the errors in the tropical upper troposphere/stratosphere to produce the realistic departure statistics. The GNSS RO departure statistics with real data tend to be larger in this region because of gravity waves (Fig. 1). The errors are inflated in the tropics by multiplying the basic error model with the function $\beta(h, \lambda)$, where λ is the latitude (radians). It must be acknowledged that the form of β used here is ad-hoc, and that it is designed simply to improve the consistency with real data. It is given by,

$$\beta(h, \lambda) = (1 + 2 \times X(\lambda) \times Y(h)) \tag{4}$$

where

$$X(\lambda) = \exp\left(-\frac{1}{2}(4\lambda)^2\right) \tag{5}$$

and,

$$Y(h) = \exp\left(1 - \frac{h - 18}{2.5} - \exp\left(-\frac{h - 18}{2.5}\right)\right) \tag{6}$$

where h is in km. This formulation leads to the largest inflation of errors at an impact height of 18 km at the equator, but it has virtually no impact in the mid-latitudes. The inflation factor is not used when assimilating the data in the EDA experiments.

Datasets containing 2000, 4000, 8000, 16000, 32000, 64000 and 128000 simulated GNSS RO bending angle profiles per day have been generated. Datasets with fewer than 128000 profiles are created from a randomly selected subset of the dataset with 128000 profiles.

The departure statistics for simulated bending angle observations have been compared against statistics of real GRAS bending angle observations (Fig. 1). The simulated observations have realistic "observed minus background" departure statistics globally – not just in the tropics, where the errors have been inflated – suggesting that the observation error specification is a reasonable approximation.

3.2 Assimilation of GNSS RO data

Simulated GNSS RO bending angle profiles are treated as real GRAS data and are assimilated with the 1D bending angle observation operator used operationally at ECMWF (Healy and Thépaut, 2006). It
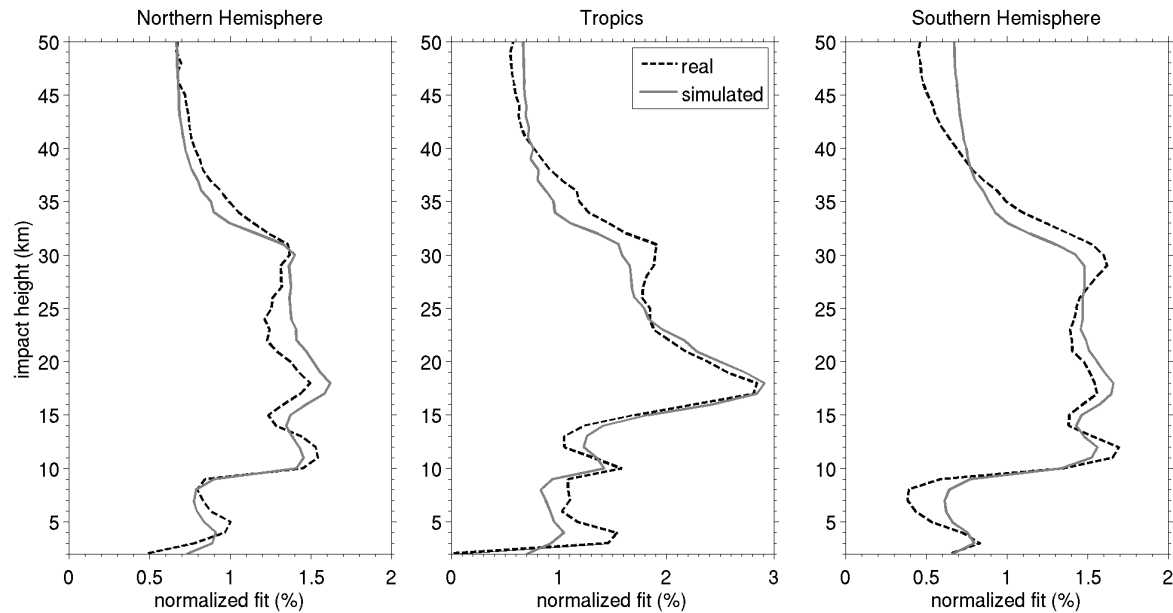
Figure 1: Standard deviations of normalized (observation – model background) values for real GRAS bending angle observations (dashed black line) and simulated GNSS RO bending angle observations (solid gray line). The results are separated for the Northern Hemisphere (left, latitude > 20°), Tropics (middle, -20° ≤ latitude ≤ 20°) and Southern Hemisphere (right, latitude < -20°) and only observations are considered that actively contribute to the analysis. Results are for the period 1-31 July 2008.

was originally assumed at the start of the study that simulating measurements with a 2D operator but then assimilating with a 1D operator would be a way of introducing realistic correlated forward model errors. However, the EDA spread values are not sensitive to this kind of inconsistency, because it is the same for every ensemble member and it cancels out when computing differences.

The geopotential heights of the model levels are evaluated in the 1D operator using the standard routines which are part of the NWP system (Simmons and Burridge, 1981), but following the work of Aparicio et al. (2009) these geopotential heights are now adjusted to account for non-ideal gas effects (Healy, 2011). As with the 2D operator, the geopotential heights are converted to geometric height with the transform given by List (1984). The geometric heights, z_g, are mapped to radius values, r, by adding the radius of curvature, R_c, and geoid undulation, u, values provided with the measurements ($r = z_g + R_c + u$), and noting that $R_c = 6371$ km and $u = 0$ km are fixed for all simulated observations.

The refractivity, N, on model levels is given by

$$N = \frac{77.643 P_d}{Z_d T} + \frac{6.3938 e}{Z_w T} + \frac{3.75463 \times 10^5 e}{Z_w T^2} \qquad (7)$$

where P_d is the pressure of dry air, e is the vapor pressure, T is the temperature and Z_d and Z_w are the dry air and water vapor compressibilities. These are the "best average" refractivity coefficients proposed by Rüeger (2002), but the $K_1 = 77.643$ K hPa^{-1} coefficient has been revised to account for its use in a formula that includes non ideal gas compressibility (Healy, 2011).

The observation operator then evaluates total ionospheric corrected bending angle, α, as a function of

---

impact parameter, a, by integrating

$$\alpha(a) \simeq -10^{-6}\sqrt{2a} \int_a^\infty \frac{\frac{dN}{dx}}{(x-a)^{1/2}} dx \tag{8}$$

where N, is the refractivity derived from the model and $x = (1 + 10^{-6}N)r$, and r is the radius value of a point on the ray-path. It is assumed that the refractivity varies exponentially with x between model levels, leading to a computation of the integral in terms of a sum of Gaussian error functions (Healy and Thépaut, 2006).

Unlike the current operational configuration at ECMWF, "tangent point drift" is not included when assimilating the GNSS RO data in the EDA experiments.

The global observation errors assumed when assimilating the GNSS RO measurements are defined as 20 % of the observed value at $h = 0$, decreasing linearly to 1 % at $h = 10$ km, and 1 % above 10 km until this reaches a lower limit of 3 microradians. These errors are used operationally at ECMWF, and they differ from the errors applied to the simulated data, which have been adjusted to provide realistic departure statistics.

3.3   Performed EDA experiments

In total nine different EDA experiments are performed for the period 1 July 2008 - 15 August 2008 (Tab. 1). Seven experiments assimilate simulated GNSS RO bending angle profiles with profile numbers increasing from 2000 per day, which is roughly what is available operationally today, to finally 128000 per day. Note that all these experiments with simulated GNSS RO profiles also assimilate all other operationally used real observations of the GOS apart from real GNSS RO profiles. So the observation impact of the current operational GOS is considered when the impact of the additional GNSS RO data is evaluated. Two additional experiments are performed that do not assimilate simulated GNSS RO profiles. An EDA experiment using real GNSS RO profiles provides a reference of the observation impact for real data and is used to demonstrate that the EDA spread with real GNSS RO observations is comparable to the spread with simulated observations. A control EDA experiment assimilating no GNSS RO data at all is applied to derive the observation impact of additional GNSS RO profiles using a GNSS RO free observing system as reference. This also enables a comparison of the GNSS RO observation impact based on the EDA approach and on traditional OSEs (Bauer et al., 2013).

The EDA experiments are performed with a version of the model cycle which was used operationally from November 2011 to July 2012 (37R3). The configuration was similar to the operational setup using a 10-member ensemble at a horizontal resolution of T399 wavenumber truncation (~ 50 km) on 91 vertical levels. The ensemble of analyses consists of 12-hourly 4D-Var data assimilation cycles, with two minimizations, at T95 and T159, respectively, and is produced twice daily at 00 UTC and 12 UTC. All EDA members use perturbed observations, sea surface fields, and model physics. The members own short-term forecasts are used to initialize the subsequent analysis cycle, so an ensemble of background states is created inside the EDA system. Note that each ensemble member uses the same static background error covariance formulation in the data assimilation. Forecasts from the ensemble of analyses are initialized once daily at 00 UTC and are computed up to +120 h at a horizontal resolution of T399. To account for model error during the forecast model integration, including the 12-hourly 4D-Var data assimilation window, model physics are perturbed using the SPPT scheme.

The EDA experiments only differ from each other in the number of assimilated GNSS RO bending angle observations. The EDA spread of the different EDA experiments determines the corresponding

name of	GNSS RO profiles	
experiment	simulated	used
EDA_ctrl	-	-
EDA_real	-	2490
EDA_2	2000	1994
EDA_4	4000	3994
EDA_8	8000	7968
EDA_16	16000	15892
EDA_32	32000	31262
EDA_64	64000	62356
EDA_128	128000	121678

Table 1: Overview of performed EDA experiments. The abbreviations of the experiments as used throughout the text are displayed. All experiments use the operationally assimilated observations of the global observing system apart from GNSS RO data unless stated otherwise. The number of profiles are the average coverage per day for the period 1 July 2008 - 15 August 2008. The 4D-Var assimilation system uses two 12-hourly assimilation windows, which means that 50 % of the profiles are effectively assimilated in each assimilation cycle.

observation impact, which is positive if the assimilation of additional GNSS RO profiles reduces the EDA spread.

4 Results of EDA experiments

4.1 Timeseries of EDA spread

Identical background fields are used to initialize the EDA experiments, and hence the ensemble requires a spin-up time of roughly one week to represent analysis and forecast error variances of the underlying NWP system correctly (Fisher et al., 2005). Figure 2 displays the time series of daily EDA spread values for +12 h forecasts of temperature averaged over the Northern Hemisphere (latitude $\geq 20°$), Tropics (-20° $\leq$ latitude $\leq$ 20°), and Southern Hemisphere (latitude $<$ -20°). The use of unperturbed identical background fields leads to initially small EDA spread values which increase within the first few days. The rate of increase is not equal for all parameters and levels, but after less than one week, all EDA spread values reach a stable state. To account for this "cold start", averaged EDA spread values (Eq. 3) are computed only for the period 8 July 2008 - 15 August 2008 excluding the initial period of seven days. The remaining period of July and August shows a small temporal variability of the EDA spread values with only minor fluctuations (Fig. 2). Averaged on a hemispheric scale, the EDA spread, which estimates the forecast error variance, does not vary as much from day to day as the forecast error. The small day-to-day variability of the hemispheric averages of the EDA spread confirms the reliability of the results, even if only a limited time period of one and a half months during a single season is considered here. The results of this study are not expected to change for a different season. An analysis of the EDA spread for the operational ECMWF model during 2011 has confirmed that the hemispherically averaged EDA spread values do not vary significantly throughout the year, and no annual signal could be detected (not shown). In fact, these results suggest that meaningful hemispherically averaged spread values could be obtained from EDA experiments of duration $\sim$ three weeks, allowing a one week spin-up period, and using the remaining two weeks for the detailed computation.
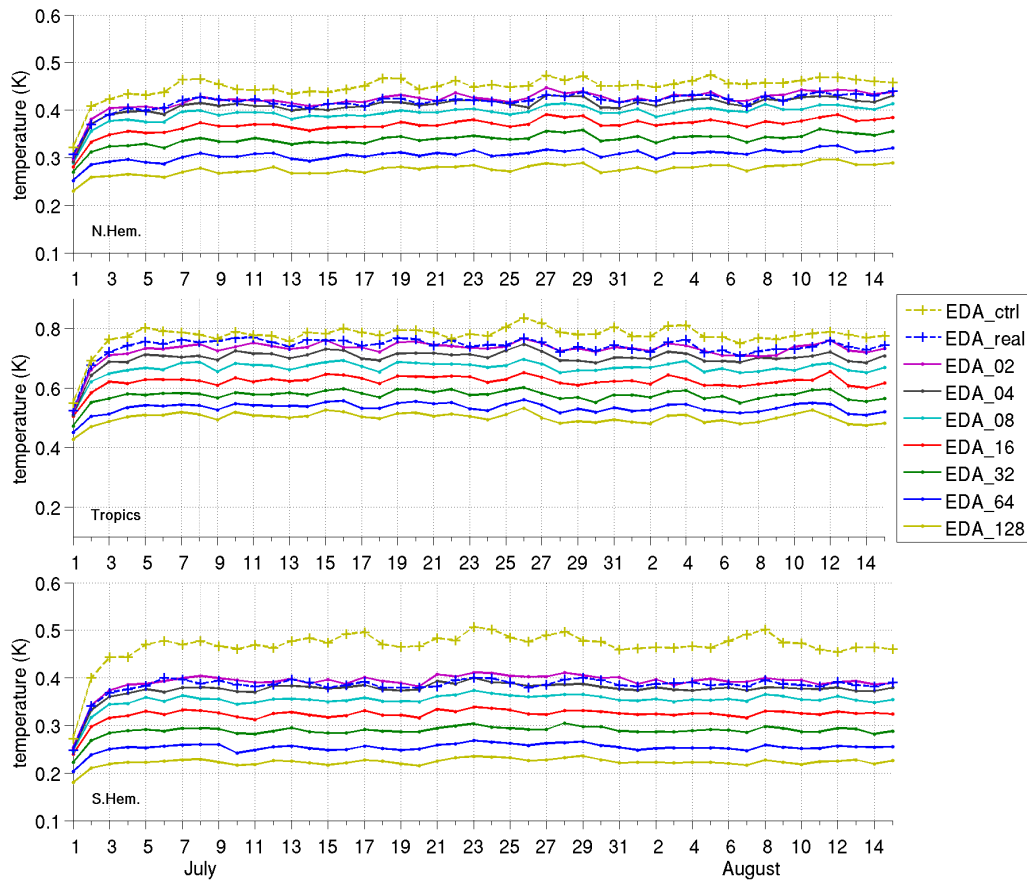
Figure 2: Time series for July - August 2008 of daily +12 h forecast EDA spread values for temperature (K) at 100 hPa.

4.2   Profiles of averaged EDA spread

In the following, averaged EDA spread values in the period 8 July 2008 - 15 August 2008 are considered. Figure 3 shows the EDA analysis spread for temperature which gives an estimate of the temperature analysis uncertainty. We focus on temperature as it is influenced most strongly by GNSS RO observations. The EDA spread values exhibit a maximum at the surface (Northern Hemisphere) or lower troposphere (Tropics, Southern Hemisphere), decrease in the middle troposphere and reach a minimum in the upper troposphere before they grow again in the stratosphere. Middle-stratospheric values are slightly smaller than the surface values in the Extratropics, but larger than surface values in the Tropics.

The EDA spread is clearly reduced when GNSS RO profiles are assimilated, and the spread values decrease as the number of simulated profiles increases (Fig. 3). The regions with the largest reduction for 2000 simulated profiles also show the largest impact for additional profiles. The additional GNSS RO profiles reduce the analysis uncertainty the most at the upper levels, particularly in the Southern Hemisphere. The uncertainty in the troposphere is also reduced but to a much smaller degree.
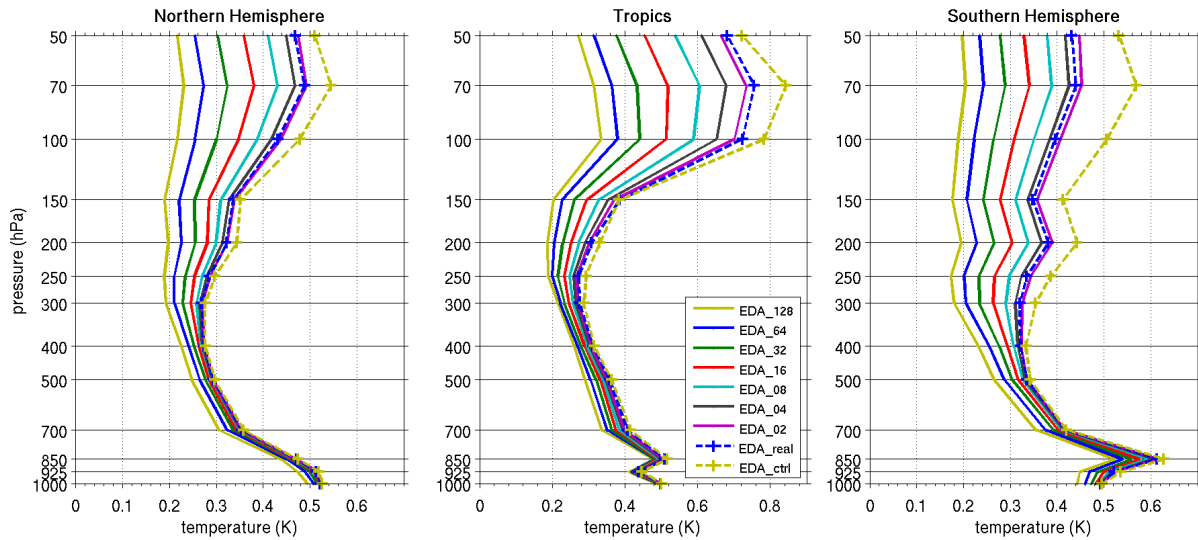
Figure 3: EDA spread for temperature (K) at analysis time averaged over the (left column) Northern Hemisphere, (middle column) Tropics and (right column) Southern Hemisphere. Results are for the period 8 July 2008 - 15 August 2008.

4.3 EDA based observation impact

As discussed in section 2, the absolute EDA spread values are prone to systematic errors and they typically underestimate the analysis and forecast uncertainty. To avoid the effect of systematic errors, the observation impact is defined as a normalized difference of EDA spread values

$$\frac{\mathrm{EDA}\_n - \mathrm{EDA\_ctrl}}{\mathrm{EDA\_ctrl}} \tag{9}$$

where EDA_n denotes the EDA spread (Eq. 3) of an experiment using a different number of GNSS RO profiles and EDA_ctrl is the EDA spread of the experiment without GNSS RO data (compare Tab. 1). The normalized spread difference accounts for the vertical variations of the uncertainty. Further, systematic errors can be neglected since they cancel out assuming similar systematic errors for the different EDA experiments. The input error statistics are the same for all EDA experiments, so systematic errors resulting from an imperfect specification of the error sources should be similar in all EDA experiments.

Figure 4 displays the observation impact (Eq. 9) on the temperature statistics for the different EDA experiments. The observation impact of EDA_real is positive (i.e. the EDA spread is reduced) and the largest impact is found between upper-tropospheric and lower-stratospheric levels. GNSS RO profiles have the largest impact in the Southern Hemisphere where conventional temperature profile observations are less frequent compared to the Northern Hemisphere. The comparison of EDA_real and EDA_2 highlights that the observation impact of real and simulated profiles in the EDA is similar. The small differences between the two experiments can be related to differences in the observational coverage, with real GNSS RO profiles having a better coverage in the Extratropics and fewer profiles in the Tropics (Fig. 5). These differences in the zonal distribution of the GNSS RO profiles lead to a larger observation impact of real data in the Extratropics and a smaller impact in the Tropics compared to 2000 simulated profiles. In addition, in the EDA_real experiment no bending angles of the GRAS instrument are assimilated actively (i.e. they do not contribute to the analysis) below 10 km in the Tropics and below 8 km in the Extratropics, which affects the impact of real data in the troposphere and leads to a more similar observation impact for EDA_real and EDA_2 in the Extratropics (Fig. 4). The screening of the real GRAS data in the lower

levels is because of the geometrical optics assumption in the processing of the data (Von Engeln et al., 2009), which is known to introduce biases.
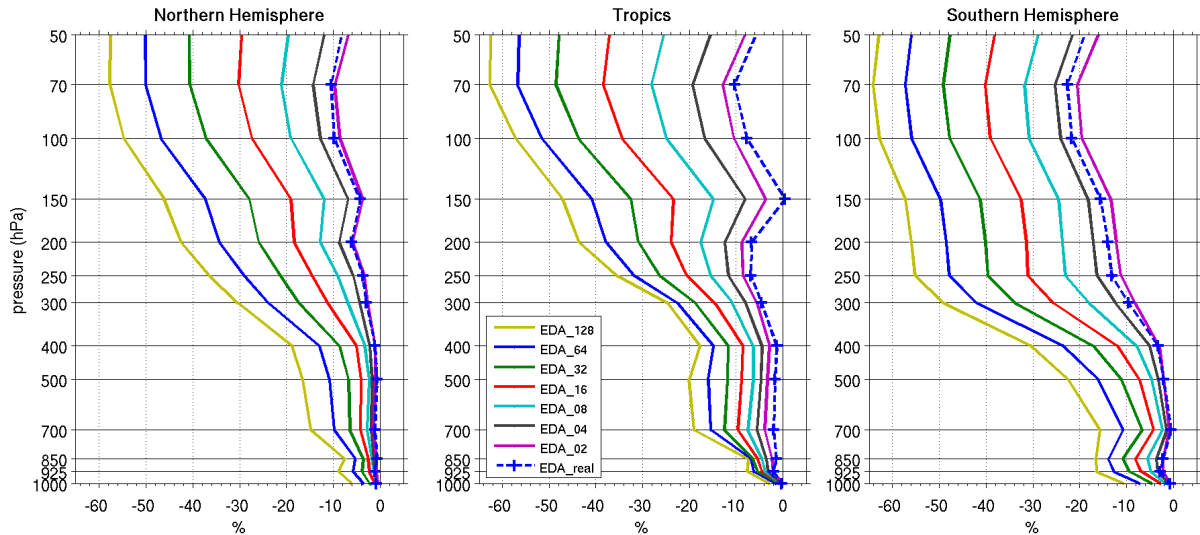

Figure 4: Normalized difference of EDA spread (%) for temperature at analysis time averaged over the (left column) Northern Hemisphere, (middle column) Tropics and (right column) Southern Hemisphere. Results are for the period 8 July 2008 - 15 August 2008.
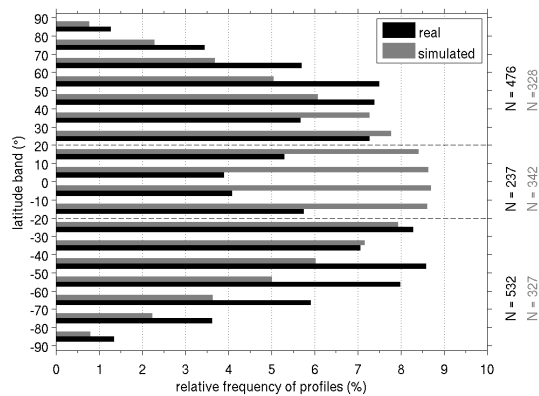

Figure 5: Zonal distribution of real (black) and simulated (gray) GNSS RO profiles in 10°-latitude bins for EDA_real (black) and EDA_2 (gray). The relative frequency with respect to the total number of 1245 for EDA_real and 997 for EDA_2 is shown. The horizontal dashed lines separates the Southern Hemisphere, from the Tropics and the Northern Hemisphere. The bending angle numbers are shown on the right side for real data (black) and simulated data (gray). Results are the average values over 00 UTC and 12 UTC assimilation cycles in the period 1 July 2008 - 15 August 2008.

Increasing the number of simulated profiles produces a gradual reduction in the normalized EDA spread values at all levels (Fig. 4). The largest impact for temperature is in the upper-troposphere and lower-/middle-stratosphere. The additional GNSS RO profiles also have a larger impact in the Southern Hemisphere than in the Northern Hemisphere. Assimilating more GNSS RO profiles always leads to a positive observation impact, and even a coverage of 128000 simulated profiles produces a reduction in the spread values when compared with 64000 profiles.
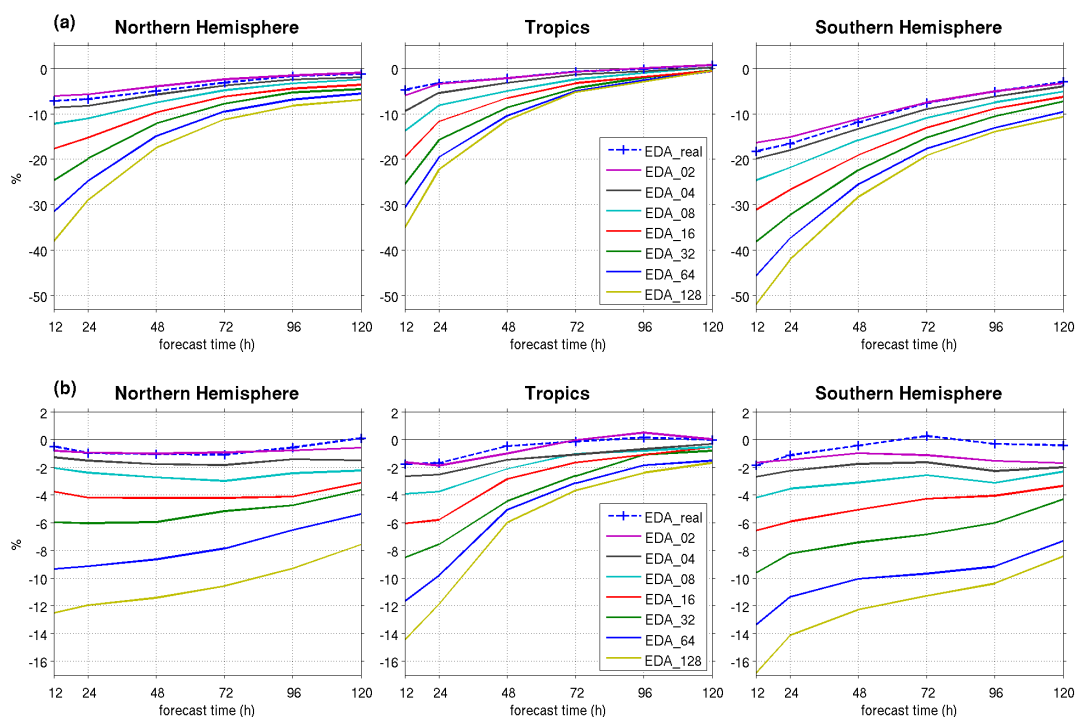
Figure 6: Normalized difference of EDA spread (%) for (a) temperature at 100 hPa and (b) geopotential height at 500 hPa at different forecast times averaged over the (left column) Northern Hemisphere, (middle column) Tropics and (right column) Southern Hemisphere. Results are for the period 8 July 2008 - 15 August 2008.

Figure 4 displays the observation impact at the analysis time, but in general the pattern of the observation impact is similar also for different forecast times. Figure 6a illustrates the evolution of the normalized EDA spread difference (Eq. 9) as function of the forecast time for temperature at 100 hPa. As the forecast time lengthens, the improvements become less significant because of sources of forecast uncertainty other than the analysis. The forecast impact on geopotential height at 500 hPa is shown in Fig. 6b. Compared to temperature at 100 hPa (Fig. 6a), the impact of the observations is much smaller and the initial improvements from additional GNSS RO profiles are reduced. However, the geopotential height improvements tend to persist longer in the Extratropics and remain nearly constant up to +120 h, especially for fewer than 32000 profiles.

4.4   Comparison with OSEs

A comprehensive set of OSEs has been performed by Bauer et al. (2013) to evaluate the impact of future developments of the space-based observing system on NWP including the impact of GNSS RO profiles. Five different experiments have been performed for the period July - September 2008. For this particular period experimental GNSS RO data from CHAMP, GRACE-A, Terrasar-X and SAC-C have been acquired in addition to the COSMIC and GRAS data that are operationally used at ECMWF. The COSMIC dataset was reprocessed, using the latest operational processing code employed at the University Corporation for Atmospheric Research (UCAR). These experiments are identical in all components of the GOS

except for the GNSS RO usage. In the control experiment, OSE_1.0, all the available GNSS RO data have been assimilated while four additional experiments, OSE_0.0, OSE_0.05, OSE_0.33 and OSE_0.67, have assimilated 0, 5, 33 and 67 % of the available GNSS RO data, respectively. These OSEs have shown that the increase of the data volume has a general positive impact on temperature and geopotential height fields, especially in the upper atmosphere (< 200 hPa), and that 100 % used GNSS RO data still produce a positive impact compared to 67 % used data (Bauer et al., 2013).

The EDA based observation impact can be compared against the observation impact derived from the OSEs of Bauer et al. (2013) to demonstrate that both methods produce a comparable observation impact of GNSS RO profiles, and the EDA approach can be used to estimate the potential impact of additional GNSS RO profiles. Forecasts of the OSEs have been evaluated for the period 8 July 2008 - 15 August 2008 and the operational ECMWF analysis has been used for verification. The standard deviation of the OSE forecast errors is considered here to make the results comparable, since the EDA spread estimates the forecast error variance and does not include changes of the mean state, which is therefore assumed to be unbiased. However, in reality this is not true and the additional GNSS RO profiles in the OSEs are likely to also affect the corresponding mean model states (e.g., Healy 2008), which leads to differences in the mean forecast errors that are not considered in the EDA approach.

The technical setup used for the OSEs and the EDA experiments is not the same. The OSEs assimilate a less extensive baseline observing system, which has been chosen to represent a possible composition of the GOS in 10 years. This means that some satellite instruments are not assimilated in the OSEs which are used in the EDA experiments. The satellite observing system in 2008 was more voluminous since many older satellites (e.g., NOAA-15) were still operating in addition to more recent platforms like NOAA-19 and Metop-A. However, it is likely that in the near future several aging satellites will not produce data anymore and the volume of the satellite data will decrease in general compared to the situation in 2008. In addition, the OSEs and EDA experiments have been performed with a different model version. While the OSEs used an older model cycle (36R4), which was operational from November 2010 to May 2011, the EDA experiments were computed with the model cycle (37R3) which was operational from November 2011 to July 2012.

The comparison of the +24 h forecast uncertainty based on the OSEs and the EDA experiments is displayed in Fig. 7. Only a subset of the EDA experiments is shown here for clarity. Note that OSE_1.0 and EDA_real assimilate the same data set of GNSS RO profiles. Despite the above mentioned differences, the vertical distribution of the forecast uncertainty is very similar for the two methods. As expected, the quantitative values of uncertainty are different as a result of the systematic error affecting the absolute EDA spread values. The EDA spread estimate is known to be too small and a temporal and spatial varying scaling factor in the order of 1-2 would account for the systematic error contribution (Bonavita et al., 2012).

Similar to the normalized difference of EDA spread (Eq. 9), a normalized error difference is computed for the OSEs taking the control experiment OSE_0.0 as reference. The normalization by the control experiment, which does not assimilate GNSS RO data, enables a one-to-one comparison of the observation impact for the two methods.

Figure 8 shows the results for temperature at +24 h forecast time. As seen before, the observation impact of real or simulated profiles agrees very well and the main observation impact is found on upper-level temperature. In the Extratropics, a small observation impact is seen for broad regions of the troposphere which grows with altitude. The EDA based observation impact is comparable to the impact in the OSEs, even if it shows slightly smaller values at all levels in the Southern Hemisphere. The smaller EDA based observation impact in the Southern Hemisphere might be related to the denser satellite observing system,
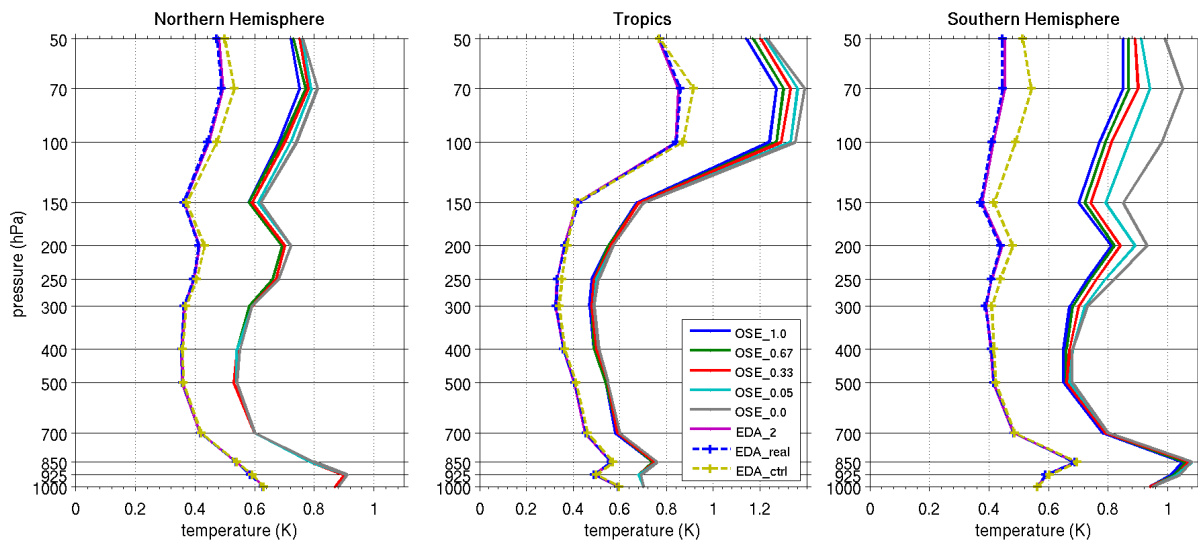
Figure 7: Standard deviation of +24 h forecast error of OSEs and +24 h forecast EDA spread for temperature (K) averaged over the (left column) Northern Hemisphere, (middle column) Tropics and (right column) Southern Hemisphere. Results are for the period 8 July 2008 - 15 August 2008.

which is likely to reduce the potential observation impact. Both methods similarly detect the largest observation impact in the Southern Hemisphere where the number of available conventional observations is smallest. A slight offset of the observation impact with a smaller EDA based impact can be identified in the Northern Hemisphere around 100 - 150 hPa. This vertical interval also shows a different observation impact in the Tropics, where it is even more pronounced. Except for these levels, the observation impact is also comparable in the Tropics, and improvements of less than 5 % in the troposphere and more than 5 % in the stratosphere can be identified. The discrepancy at tropopause height might be related to the different model versions used for the EDA experiments and the OSEs. The tropical regions are particularly prone to model biases with a changing sign at tropopause level, and these model deficiencies are affected by improvements applied to convection and cloud parametrization between different model versions. In addition, the differences at tropopause level might again be related to the denser satellite observational network used in the EDA experiments.

The comparison of the observation impact for geopotential height shows similar results (not shown). Unlike the temperature results, a slight offset of the observation impact is found in the tropical troposphere, with a larger EDA based observation impact. However, one has to consider that the verification of OSEs is also sensitive to the choice of the reference analysis and verifying OSE_1.0 with its own analysis produces a larger observation impact in the Tropics. In regions with larger model errors, like the Tropics and the stratosphere in general, the sensitivity to the reference analysis leads to an uncertainty in the OSE observation impact which is as large as the difference between the observation impact based on the OSEs and EDA experiments.

Figure 9 compares the scaling of the observation impact for +24 h temperature forecasts in the OSEs using real GNSS RO profiles and in the EDA experiments using up to 8000 simulated profiles per day. A 100 % GNSS RO coverage corresponds to an average number of 2450 GNSS RO profiles, which is slightly larger than the 2000 simulated profiles used in EDA_2. Additionally, the zonal distribution of real and simulated profiles is different (Fig. 5), which has to be considered here for the direct comparison of 100 % GNSS RO coverage and 2000 simulated profiles. As shown in Fig. 8, the observation impact of 2000 simulated profiles derived from the EDA spread is comparable to the impact of full coverage
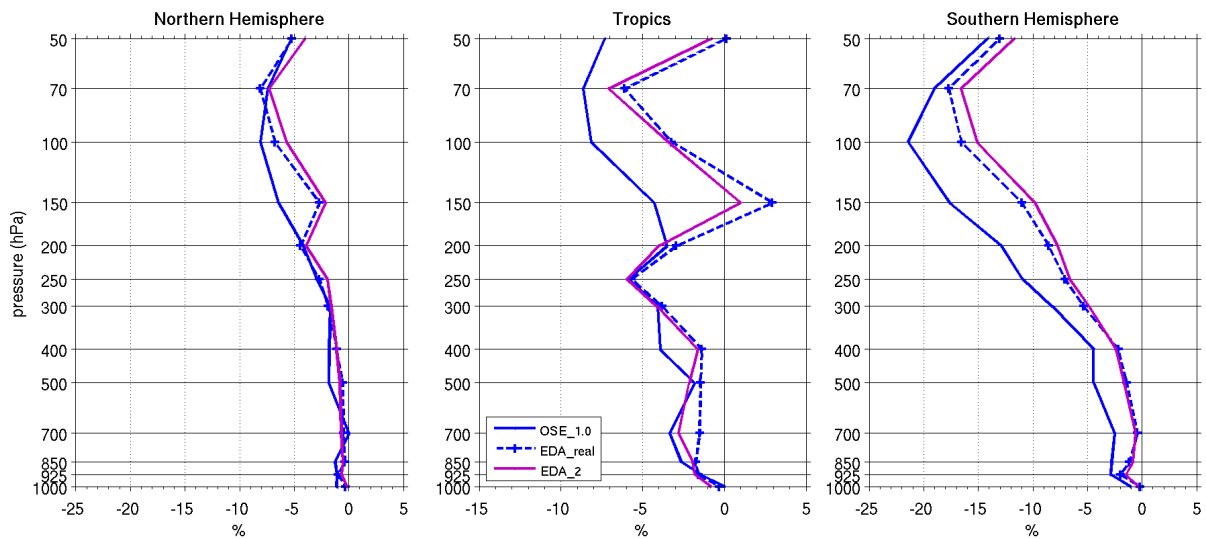
Figure 8: Normalized difference (%) of standard deviation of +24 h forecast error of OSEs and +24 h forecast EDA spread for temperature averaged over the (left column) Northern Hemisphere, (middle column) Tropics and (right column) Southern Hemisphere. Results are for the period 8 July 2008 - 15 August 2008.

of real profiles in the OSEs. EDA based improvements are generally smaller than what is found with the OSEs, but the shape of the scaling curve looks very similar and no saturation has been reached at the currently available observational coverage. The EDA approach is able to extend the curve of the observation impact for additional simulated GNSS RO profiles and significant improvements can still be identified for more profiles. Note that the EDA based observation impact is only limited to 8000 profiles in Fig. 9 to enable the comparison of OSE and EDA results.
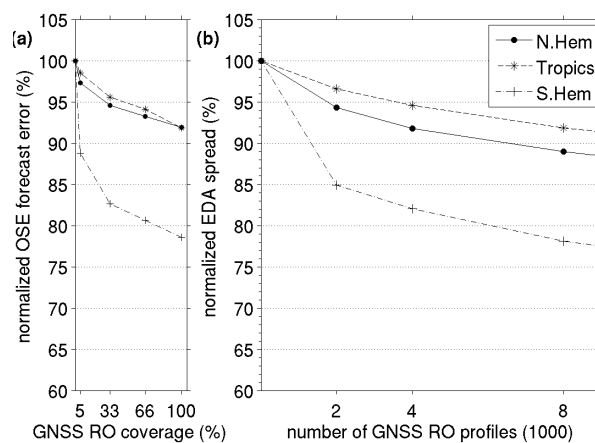

Figure 9: (a) Normalized standard deviation of +24 h forecast error of OSEs as function of the assimilated percentage of GNSS RO data and (b) normalized EDA spread (%) at +24 h forecast time as function of the assimilated number of simulated GNSS RO profiles. Results are for temperature at 100 hPa for the period 8 July 2008 - 15 August 2008.

In summary, the observation impact of GNSS RO profiles found with OSEs is comparable to the EDA based impact, considering the uncertainties related to the choice of the reference analysis, the used model version and the differences in the baseline GOS. Hence, this suggests the EDA based observation impact

is able to produce a realistic approximation of the observation impact, and predicting the potential observation impact of an increased observational coverage beyond the current number of 2000-3000 profiles per day appears reasonable.

4.5 Scaling of the observation impact

Figure 10 displays the scaling of the observation impact for up to 128000 simulated GNSS RO profiles at the analysis time. The EDA spread is normalized with EDA_ctrl and the improvements are relative to using no GNSS RO data. Increasing the data coverage above the current available number of ~ 2000 profiles leads to significant improvements, which emphasizes the potential benefits of additional GNSS RO profiles. Considering the impact on temperature for up to 16000 profiles, one can see that below 500 hPa the spread is only reduced by less than 10 % for the Tropics and Southern Hemisphere, and less than 5 % for the Northern Hemisphere. Above 500 hPa, the EDA spread is reduced by 20-30 % for the Northern Hemisphere, 25-35 % for the Tropics and 30-40 % for the Southern Hemisphere. The largest impact on temperature and geopotential height is always located in the Southern Hemisphere while the impact on low-level relative humidity is more pronounced in the Northern Hemisphere and the Tropics.
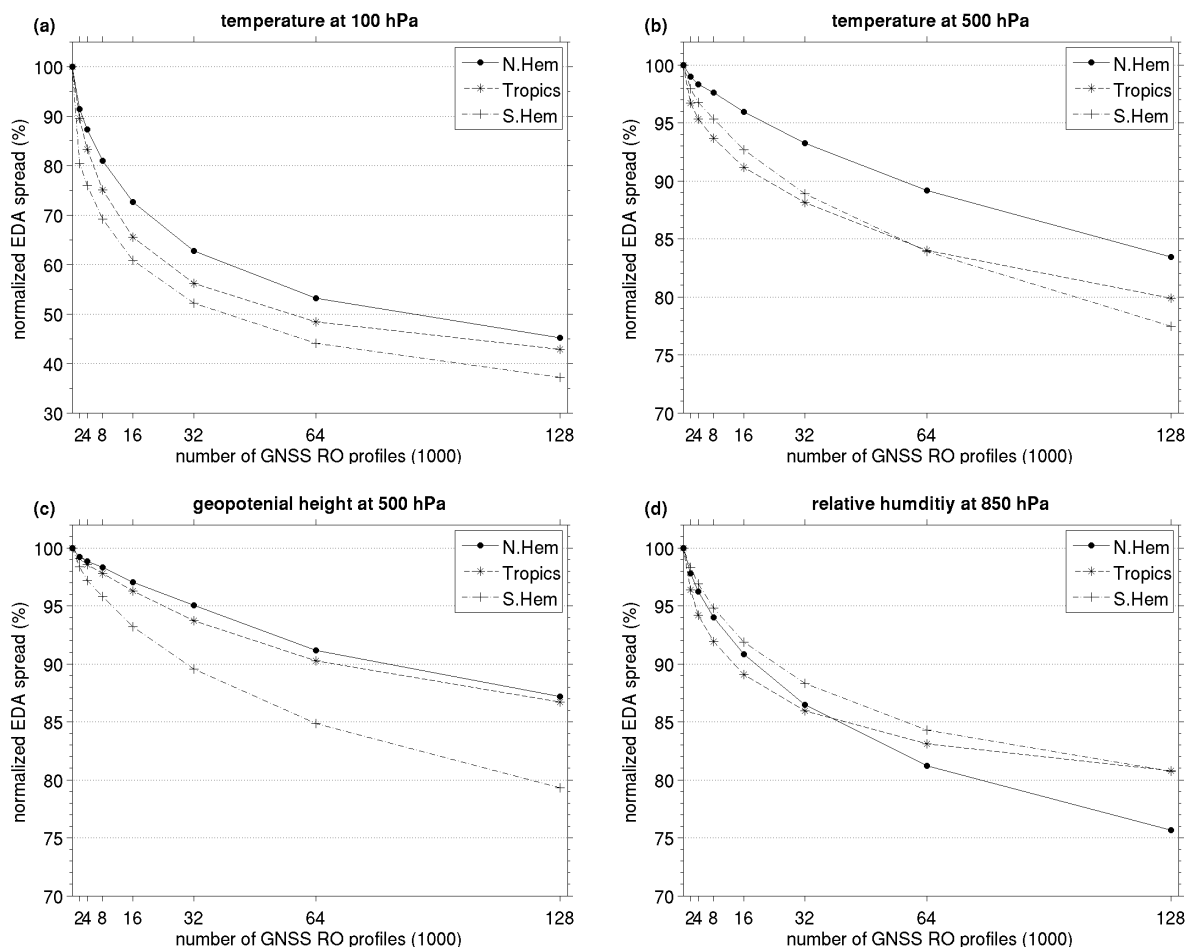

Figure 10: Normalized EDA spread (%) at analysis time as function of the assimilated number of simulated GNSS RO profiles for (a) temperature at 100 hPa, (b) temperature at 500 hPa, (c) geopotential height at 500 hPa and (d) relative humidity at 850 hPa. Results are for the period 8 July 2008 - 15 August 2008.

Spread reductions resulting from a doubling of the profile number are always evident, but they become smaller in a fractional sense as the data numbers increase. The improvement gained with 16000 profiles accounts in general for around 50 % or more of the improvement achieved with 128000 profiles at the vertical levels where GNSS RO data show a significant impact. All results clearly show that the EDA spread is continuously reduced for large observation numbers, and even with the maximum coverage of 128000 profiles per day we do not see a "zero improvement" threshold. Hence, zero spread reduction can not be used to define "saturation" of the observation impact in this study.

Only the results for the observation impact at analysis time are shown here, but the general shape of the scaling curve is similar for different forecast times.

5 Discussion

The focus of this study was to evaluate the impact of significantly increasing the number of GNSS RO profiles, and it was done using simulated GNSS RO data. The comparison of the EDA spread based observation impact of real and a comparable number of simulated GNSS RO profiles shows a very good agreement, suggesting the EDA spread can be applied to estimate the impact of simulated data. The EDA based observation impact for real and simulated GNSS RO profiles is positive, and the largest improvements are seen for upper-tropospheric/lower-stratospheric levels. The impact is largest in the Southern Hemisphere where conventional temperature profile observations are less abundant compared with the Northern Hemisphere. These results are consistent with previous studies evaluating the theoretical information content of GNSS RO data (e.g., Collard and Healy 2003) or the Forecast Sensitivity to Observation (Cardinali and Healy, 2011). Additionally, a comparison with OSEs (Bauer et al., 2013) confirmed that the EDA approach can be applied to derive the observation impact of GNSS RO profiles. Increasing the number of observations amplifies the observation impact especially in the regions where already a positive impact was found with lower data coverage, and the uncertainty was continuously reduced for additional observations.

However, it has to be noted that using simulated observations does not lead to an improved model state estimate, even though the EDA spread based error variance estimate is reduced. The simulated observations contain information from NWP model analysis used in the simulation, which in turn depends on the GOS used to estimate that analysis. When the simulated observations are re-assimilated together with real observations of the GOS in the EDA experiments, they are treated as if they provide new information, which is clearly not the case. This leads to a sub-optimality in the data assimilation since observation errors, which are assumed to be uncorrelated, are actually correlated. Each single analysis does not represent an optimal solution to the assimilation problem anymore, and is likely to be degraded when simulated GNSS RO profiles are assimilated. Simulating data from a model analysis created with a different NWP system does not fully avoid this problem since all NWP models assimilate broadly the same information from the GOS. A simple linear problem is shown in Appendix B that illustrates the difficulty of mixing real and simulated observations in the data assimilation. The negative effect of assimilating a set of simulated GNSS RO observations on top of the other observations of the GOS can clearly be identified in the forecasts of the EDA mean, and we have found that increasing the number of simulated profiles can degrade the state estimate (not shown).

Although quality or skill of the EDA mean state and each single EDA member is affected by assimilating both real and simulated data, the EDA spread is not. Similar to an EnKF framework, the EDA method solves the equations for the model state, but uses the ensemble of model states to construct the error statistics separately. The EDA spread represents the analysis (forecast) error variance estimate, which

is constructed from all EDA members (Eqs. (1) and (2)), and it is a function of perturbations added to observations and the model state, and the static background error covariance matrix used in the assimilation. There may be certain degree of mis-specification in the assumed static background error covariance matrix used in the EDA approach, but fortunately the spread values we compute do not rely on the use of an optimal gain matrix (Appendix A), so the use of a sub-optimal static background error covariance matrix is not important in the results presented here. Therefore, the spread values will provide useful information, given that the observation and model perturbations, calculated from the assumed error covariance matrices of the observations, $\mathbf{R}$, and the model, $\mathbf{Q}$, respectively, are realistic.

The SPPT approach accounting for model error is well established (Palmer et al., 2009), and it is used operationally at ECMWF (Buizza et al., 1999). The GNSS RO profiles are assimilated with the observation error covariance matrix model currently used operationally at ECMWF. This matrix must be a reasonable approximation, given the impact of the GNSS RO data in the ECMWF system, but it is diagonal, neglecting both vertical and horizontal error correlations. It is has been shown in simulation studies that neglecting horizontal correlations can lead to over optimistic results (Liu and Rabier, 2003). However, even at a data volume of 128000 GNSS RO profiles per day, there is still a mean horizontal spacing of about 300 km per hour, assuming spatially and temporally randomly distributed profiles, and this mean separation doubles to 600 km for 32000 randomly spaced profiles. Therefore, we do not expect that the chosen coverage of simulated GNSS RO profiles leads to significant error correlations. Furthermore, improved 2D observation operators are currently under development (Healy et al., 2007), and these should mitigate the impact of any horizontally correlated forward model errors.

No objectively defined "saturation" level of the observation impact could be detected as a result of the continuous reductions in the EDA spread values as the number of GNSS RO profiles increased. Once the link between the EDA spread values and the theoretical error statistics is acknowledged, this result is an obvious consequence of standard variational data assimilation/retrieval theory. Highly correlated observations with uncorrelated errors will always reduce the theoretical analysis/retrieval errors, even if the additional measurements do not effectively add new information to the NWP system. This is a result of reducing random measurement noise by repetition (Twomey, 1977). Exactly the same arguments apply to the EDA system. Even though additional measurements might not contain significant new information, they can reduce the spread values of the system by effectively reducing measurement noise through repetition, as long as uncorrelated observation errors are assumed. We have investigated if the ongoing reduction of the EDA spread at large observation numbers is just because the additional observations are repetitions of the previous measurements. It is possible to construct a simple $\sqrt{n}$-type fitting function which approximates the EDA spread of 128000 profiles, using the EDA spread results of 32000 and 64000 profiles as input. This would suggest that the improvements beyond 32000 profile result generally result from repeating the measurements, and not from new information brought to the NWP system. However, an additional EDA experiment was performed using 64000 profiles, but doubling the assumed observation error variances. We found that the 64000 "degraded" observations produced lower spread values than the standard EDA_32 experiment, indicating that even at this dense coverage new information can still be extracted from the additional GNSS RO profiles.

One characteristic of GNSS RO measurements that has not been investigated in the EDA experiments is the ability to reduce biases, and "anchor" the bias corrections applied to radiance measurements. This is because the EDA spread values provide information about the random component of the error statistics. It may be possible to design an experiment where the GNSS RO are deliberately biased, to investigate how the model state is pulled towards the GNSS RO measurements as the numbers are increased, but this will have to be investigated in future work.

6 Summary and conclusions

This study was designed to investigate the GNSS RO impact as a function of observation number. The objectives were to determine how the impact of the data scales with the number of observations, and to identify if there is an apparent saturation limit of the observational impact. Future GNSS RO observation volumes were accounted for by simulating the observations from reference model runs. A dataset of up to 128000 simulated GNSS RO profiles per day was generated for a six week period in summer 2008. The GNSS RO profiles were produced from operational ECMWF analyses using a 2D bending angle operator (Healy et al., 2007), and realistic departure statistics were obtained after adding random errors.

A comprehensive set of nine EDA experiments have been performed with different numbers of simulated GNSS RO profiles that were assimilated in addition to the other real measurements provided the GOS. The spread of the EDA analyses and forecasts yields a statistical estimate of the analysis and forecast uncertainty of the NWP model as a function of GNSS RO observation number, and this was used to determine the corresponding observation impact. The EDA spread is not affected by using simulated instead of real observations. However, it has to be considered that the EDA spread will only correctly describe the uncertainty of the underlying NWP system if the observations, model and external boundaries are perturbed with realistic error estimates. The observation impact for GNSS RO profiles based on the EDA spread generally agrees with the impact found in OSEs. This indicates that the EDA spread is able to produce a realistic estimate of the observation impact for GNSS RO data.

The EDA spread based observation impact of the simulated data was found to be largest at analysis time and gradually decreased for longer forecast times up to day 5. No forecasts after day 5 were considered in this study. Consistent with results from previous OSE studies (Poli et al., 2008; Bauer et al., 2013) the largest impact of GNSS RO observations was seen for temperature from the upper-troposphere to the middle-stratosphere in the Southern Hemisphere. The observation impact of using real GNSS RO observations compared to 2000 simulated profiles in the EDA showed a very good agreement, and the differences were linked mainly to the different coverage with RO profiles. For the simulated data, we assumed that the profile locations are randomly distributed on the sphere, which produced a higher data density in the Tropics, and a less dense coverage in the Extratropics when compared with real data.

The increase of observation numbers had a positive impact on the analysis (forecast) uncertainty, which was largest in the regions where the real data has the largest impact. The upper-levels see the largest improvements from additional data, especially in the Southern Hemisphere and over the tropical oceans where conventional observations are relative sparse. Large profile numbers also led to improvements in the middle-/lower-troposphere, but in general the impact of GNSS RO data remained much smaller here compared to the upper levels of the atmosphere.

The impact of GNSS RO data was analyzed as a function of the GNSS RO profile number, to derive information on the scaling of the observation impact. It is clear that the impact per observation on the spread values falls as the number of observations increases. However, there is still an additional benefit of going to 32000, 64000 and 128000 profiles per day, as the EDA spread values continue to be reduced. There is no "saturation" of the observation impact, in terms of a zero observation impact with the EDA approach used here, but this is a well known consequence of assuming uncorrelated observation errors. In general, it has been found that $\sim$ 16000 profiles generally account for around 50 % or more of the improvements achieved with 128000 profiles, assuming that the profiles are randomly distributed in time and space on the sphere. With consideration for the relatively coarse sampling of the GNSS RO observation numbers used in this study, we suggest the results support a number in the region of 16000 to 20000 globally distributed observations per day, as a minimum observational coverage for the GNSS RO component of the future GOS. To achieve this coverage requires GNSS RO instruments with the capability

to measure both GPS and Galileo signals on around 16 to 20 LEO satellites.

To confirm and refine the results presented here, we would encourage future studies comparing OSSEs with the EDA approach.

Acknowledgements

Appendix A

Theoretical justification of the EDA method

The EDA method is described in detail in Žagar *et al.* (2005) and Isaksen *et al.* (2010b), but a brief summary is presented here for clarification of the results.

Consider the general linear analysis-forecast system

$$\mathbf{x}_a^k = \mathbf{x}_b^k + \mathbf{K}_k \left(\mathbf{y}^k - \mathbf{H}_k \mathbf{x}_b^k \right) \tag{10}$$

$$\mathbf{x}_b^{k+1} = \mathbf{M}_k \mathbf{x}_a^k \tag{11}$$

where k denotes the analysis time, $\mathbf{y}^k$ the observation vector, $\mathbf{x}_b^k$ the model background state and $\mathbf{x}_a^k$ the model analysis state. $\mathbf{M}_k$ and $\mathbf{K}_k$ are matrices describing the model forecast and a general gain matrix, respectively, and $\mathbf{H}_k$ is the observation operator. There is no assumption of optimality, and more specifically $\mathbf{K}_k$ is not required to be the Kalman gain matrix.

Assuming that observation, background and model errors are independent of each other, the analysis and background error covariance matrices, $\mathbf{P}_k^a$ and $\mathbf{P}_k^b$, respectively, can be shown to evolve according to

$$\mathbf{P}_k^a = (\mathbf{I} - \mathbf{K}_k \mathbf{H}_k) \mathbf{P}_k^b (\mathbf{I} - \mathbf{K}_k \mathbf{H}_k)^T + \mathbf{K}_k \mathbf{R}_k \mathbf{K}_k^T \tag{12}$$

$$\mathbf{P}_{k+1}^b = \mathbf{M}_k \mathbf{P}_k^a \mathbf{M}_k^T + \mathbf{Q}_k \tag{13}$$

where $\mathbf{R}_k$ is the covariance matrix for the observation error and $\mathbf{Q}_k$ for the model error. Since we do not assume the Kalman gain matrix, $\mathbf{P}_k^a$ is not generally the optimal, minimum variance solution. Furthermore, in this linear system the error statsistics do not depend on the observation values.

For a perturbed analysis-forecast system using perturbed observations, $\mathbf{y}^k + \eta^k$, and a stochastic forcing term that represents model errors, ζ^k, the general equations (Eqs. (10) and (11)), can be written as

$$\tilde{\mathbf{x}}_a^k = \tilde{\mathbf{x}}_b^k + \mathbf{K}_k \left(\mathbf{y}^k + \eta^k - \mathbf{H}_k \tilde{\mathbf{x}}_b^k \right) \tag{14}$$

$$\tilde{\mathbf{x}}_b^{k+1} = \mathbf{M}_k \tilde{\mathbf{x}}_a^k + \zeta^k \tag{15}$$

where $\tilde{\mathbf{x}}_a^k$ and $\tilde{\mathbf{x}}_b^{k+1}$ are the perturbed analysis and background states, respectively.

The differences between the perturbed and unperturbed states leads to the equations for the perturbations

$$\varepsilon_a^k = \tilde{\mathbf{x}}_a^k - \mathbf{x}_a^k = \varepsilon_b^k + \mathbf{K}_k \left(\eta^k - \mathbf{H}_k \varepsilon_b^k \right) \tag{16}$$

$$\varepsilon_b^{k+1} = \tilde{\mathbf{x}}_b^{k+1} - \mathbf{x}_b^{k+1} = \mathbf{M}_k \varepsilon_a^k + \zeta^k \tag{17}$$

which implies that the perturbations evolve with the same update equations and matrices as in the general unperturbed case (Eqs. (10) and (11)).

The covariance matrices for the perturbations of the analysis and background state are given by

$$\overline{\varepsilon_a^k \left(\varepsilon_a^k \right)^T} = (\mathbf{I} - \mathbf{K}_k \mathbf{H}_k) \overline{\varepsilon_b^k \left(\varepsilon_b^k \right)^T} (\mathbf{I} - \mathbf{K}_k \mathbf{H}_k)^T + \mathbf{K}_k \mathbf{R}_k \mathbf{K}_k^T \tag{18}$$

$$\overline{\varepsilon_b^{k+1} \left(\varepsilon_b^{k+1} \right)^T} = \mathbf{M}_k \overline{\varepsilon_a^k \left(\varepsilon_a^k \right)^T} \mathbf{M}_k^T + \mathbf{Q}_k \tag{19}$$

where the applied perturbations η^k and ζ^k are required to have the error covariance matrices $\mathbf{R}_k$ and $\mathbf{Q}_k$, respectively. From the comparison with Eqs. (12) and (13) it can be seen that if $\overline{\varepsilon_b^k \left(\varepsilon_b^k\right)^T} = \mathbf{P}_k^b$ at some time k, $\overline{\varepsilon_a^k \left(\varepsilon_a^k\right)^T} = \mathbf{P}_k^a$ and $\overline{\varepsilon_b^{k+1} \left(\varepsilon_b^{k+1}\right)^T} = \mathbf{P}_{k+1}^b$. This implies that the error statistics of the analysis-forecast system can be generated from an ensemble of perturbed assimilation cycles.

Appendix B

Assimilating a mixture of real and simulated data

Consider the simple linear analysis system, designed to illustrate the difficulty assimilating both real and simulated data. We assimilate the real data $\mathbf{y}$,

$$\mathbf{x}_a = \mathbf{x}_b + \mathbf{K}\left(\mathbf{y} - \mathbf{H}\mathbf{x}_b\right) \tag{20}$$

The analysis, $\mathbf{x}_a$, is then used to simulate observations $\mathbf{y}_s$

$$\mathbf{y}_s = \mathbf{H}_s \mathbf{x}_a + \varepsilon_s \tag{21}$$

including random noise ε_s. Now using the original background state, assimilate both real and simulated observations. If simulated and real observations are assumed to have uncorrelated observation errors, this can be done in two steps, with the first step simply reproducing Eq. (20) and the second step

$$\mathbf{x}_{a,s} = \mathbf{x}_a + \mathbf{K}_s\left(\mathbf{y}_s - \mathbf{H}_s \mathbf{x}_a\right) = \mathbf{x}_a + \mathbf{K}_s \varepsilon_s \tag{22}$$

This demonstrates that the assimilation of simulated and real observations produces an additional noise term in the new analysis $\mathbf{x}_{a,s}$.

References

Anthes, R., et al., 2008: The COSMIC/FORMOSAT-3 Mission: Early Results. *Bull. Amer. Meteor. Soc.*, **89**, 313–333.

Aparicio, J. and G. Deblonde, 2008: Imapct of the assimilation of CHAMP refractivity profiles in Environment Canada Global Forecasts. *Mon. Wea. Rev.*, **136**, 257–275.

Aparicio, J., G. Deblonde, L. Garand, and S. Laroche, 2009: The signature of the atmospheric compressibility factor in COSMIC, CHAMP and GRACE radio occultation data. *J. Geophys. Res.*, **114**, doi:10.1029/2008JD011 156.

Auligné, T., A. McNally, and D. Dee, 2007: Adaptive bias correction for satellite data in a numerical weather prediction system. *Quart. J. Roy. Meteorol. Soc.*, **133**, 631–642. doi: 10.1002/qj.56.

Bauer, P., G. Radnoti, S. Healy, and C. Cardinali, 2013: GNSS radio occultation constellation observing system experiments. *submitted to Mon. Wea. Rev.*

Beyerle, G., et al., 2011: First results from the GPS atmosphere sounding experiment TOR aboard the TerraSAR-X satellite. *Atmos. Chem. Phys.*, **11**, 6687–6699.

Bonavita, M., L. Isaksen, and E. Hólm, 2012: On the use of EDA background error variances in the ECMWF 4D-Var. *Quart. J. Roy. Meteorol. Soc.*, **138**, 1540–1559.

Bonavita, M., L. Raynaud, and L. Isaksen, 2011: Estimating background-error variances with the ECMWF Ensemble of Data Assimilations system: some effects of ensemble size and day-to-day variability. *Quart. J. Roy. Meteorol. Soc.*, **137**, 423–434.

Bormann, N., S. Saarinen, G. Kelly, and J. Thépaut, 2003: The spatial structure of observation errors in atmospheric motion vectors from geostationary satellite data. *Mon. Wea. Rev.*, **131**, 706–718.

Buizza, R., M. Leutbecher, L. Isaksen, and J. Haseler, 2010a: Combined use of EDA- and SV-based perturbations in the EPS. *ECMWF Newsletter*, Vol. 123, 22–28.

Buizza, R., M. Miller, and T. Palmer, 1999: Stochastic representation of model uncertainties in the ECMWF ensemble prediction system. *Quart. J. Roy. Meteorol. Soc.*, **125**, 2887–2908.

Burgers, G., P. Jan van Leeuwen, and G. Evensen, 1998: Analysis scheme in the ensemble Kalman filter. *Mon. Wea. Rev.*, **126**, 1719–1724.

Cardinali, C. and S. Healy, 2011: GPS-RO at ECMWF. *Proc. ECMWF Seminar of Data Assimilation for atmosphere and ocean, 6 - 9 September 2011*, Reading, UK, ECMWF, 323–336.

Collard, A. and S. Healy, 2003: The combined impact of future space-based atmospheric sounding instruments on numerical weather-prediction analysis fields: A simulation study. *Quart. J. Roy. Meteorol. Soc.*, **129**, 2741–2760.

Cucurull, L., 2010: Improvement in the use of an operational constellation of GPS radio occultation receivers in weather forecasting. *Wea. Forecasting*, **25**, 749–767.

Eyre, J., 1989: Inversion of cloudy satellite sounding radiances by nonlinear optimal estimation. I: Theory and simulation for TOVS. *Quart. J. Roy. Meteorol. Soc.*, **115**, 1001–1026.

Eyre, J., 1990: The information content of data from satellite sounding systems: A simulation study. *Quart. J. Roy. Meteorol. Soc.*, **116**, 401–434.

Fisher, M., M. Leutbecher, and G. Kelly, 2005: On the equivalence between Kalman smoothing and weak-constraint four-dimensional variational data assimilation. *Quart. J. Roy. Meteorol. Soc.*, **131**, 3235–3246.

Healy, S., 2008: Forecast impact experiment with a constellation of GPS radio occultation receivers. *Atmospheric Science Letters*, **9**, 111–118.DOI: 10.1002/asl.169.

Healy, S., 2011: Refractivity coefficients used in the assimilation of GPS radio occultation measurements. *J. Geophys. Res.*, **116**, doi:10.1029/2010JD014 013.

Healy, S., J. Eyre, M. Hamrud, and J.-N. Thépaut, 2007: Assimilating GPS radio occultation measurements with two-dimensional bending angle observation operators. *Quart. J. Roy. Meteorol. Soc.*, **133**, 1213–1227.

Healy, S. and J.-N. Thépaut, 2006: Assimilation experiments with CHAMP GPS radio occultation measurements. *Quart. J. Roy. Meteorol. Soc.*, **132**, 605–623.

Isaksen, L., M. Bonavita, R. Buizza, M. Fisher, J. Haseler, M. Leutbecher, and L. Raynaud, 2010b: Ensemble of Data Assimilations at ECMWF. Tech. Rep. ECMWF RD Tech. Memo. 636, 45 pp.

Isaksen, L., M. Fisher, and J. Berner, 2007: Use of analysis ensembles in estimating flow-dependent background error variance. *Proc. ECMWF workshop on Flow-dependent aspects of data assimilation, 11 - 13 June 2007*, Reading, UK, ECMWF, 65–86.

Isaksen, L., J. Haseler, R. Buizza, and M. Leutbecher, 2010a: The new Ensemble of Data Assimilations. *ECMWF Newsletter*, Vol. 123, 17–21.

Kursinski, E., et al., 1996: Initial results of radio occultation observations of earth's atmosphere using the Global Positioning System. *Science*, **271**, 1107–1110.

Leutbecher, M., 2009: Diagnosis of ensemble forecasting systems. *Proc. ECMWF Seminar on Diagnosis of Forecasting and Data Assimilation Systems, 7 - 10 September 2009*, Reading, UK, ECMWF, 235–266.

List, R., (Ed.) , 1984: *Smithsonian meteorological tables*. Smithsonian Institution Press, Washington.

Liu, Z.-Q. and F. Rabier, 2003: The potential of high-density observations for numerical weather prediction: A study with simulated observations. *Quart. J. Roy. Meteorol. Soc.*, **129**, 3013–3035.

Luntama, J.-P., et al., 2008: Prospects of the EPS GRAS Mission for Operational Atmospheric Applications. *Bull. Amer. Meteor. Soc.*, **89**, 1863–1875.

Masutani, M., et al., 2010: Observing System Simulation Experiments. *Data Assimilation: Making sense of observations*, B. K. W. Lahoz and R. Ménard, Eds., Springer, 647–679.

Palmer, T., R. Buizza, F. Doblas-Reyes, T. Jung, M. Leutbecher, G. Shutts, M. Steinheimer, and A. Weisheimer, 2009: Stochastic parametrization and model uncertainty. Tech. Rep. ECMWF RD Tech. Memo. 598, 42 pp.

Poli, P., S. Healy, F. Rabier, and J. Pailleux, 2008: Preliminary assessment of the scalability of GPS radio occultations impact in numerical weather prediction. *Geophys. Res. Lett.*, **35 (23)**, L23 811, doi:10.1029/2008GL035 873.

Rabier, F., N. Fourrié, D. Chafäi, and P. Prunet, 2002: Channel selection methods for infrared atmospheric sounding interferometer radiances. *Quart. J. Roy. Meteorol. Soc.*, **128**, 1011–1027.

Raynaud, L., L. Berre, and G. Desroziers, 2009: Objective filtering of ensemble-based background-error variances. *Quart. J. Roy. Meteorol. Soc.*, **135**, 1177–1199.

Rennie, M. P., 2010: The impact of GPS radio occultation assimilation at the Met Office. *Quart. J. Roy. Meteorol. Soc.*, **136**, 116–131.

Rocken, C., et al., 1997: Analysis and validation of GPS/MET data in the neutral atmosphere. *J. Geophys. Res.*, **102**, 29.849–29.866.

Rodgers, C., 2000: *Inverse methods for atmospheric sounding: Theory and practice*. World Scientific Publishing, Singapore, New Jersey, London, Hong Kong.

Rüeger, J., 2002: Refractive index formulae for electronic distance measurements with radio and millimetre waves. Unisurv Report 68, 1–52 pp., School of Surveying and Spatial Information Systems, University of New South Wales.

Simmons, A. and D. Burridge, 1981: An energy and angular momentum conserving vertical finite difference scheme and hybrid coordinate. *Mon. Wea. Rev.*, **109**, 758–766.

Tan, D. G. H., E. Andersson, M. Fisher, and I. Isaksen, 2007: Observing-system impact assessment using a data assimilation ensemble technique: application to the ADM-Aeolus wind profiling mission. *Quart. J. Roy. Meteorol. Soc.*, **133**, 381–390.

Twomey, S., 1977: *Introduction to Mathematics of Inversion in Remote Sensing and Indirect Measurements*. Elsevier Scientific Publishing, Amsterdam, 243 pp.

Vialard, J., F. Vitart, M. Balmaseda, T. Stockdale, and D. Anderson, 2005: An ensemble generation method for seasonal forecasting with an ocean-atmosphere coupled model. *Mon. Wea. Rev.*, **133**, 441–453.

Von Engeln, A., S. Healy, C. Marquardt, Y. Andres, and F. Sancho, 2009: Validation of operational GRAS radio occultation data. *Geophys. Res. Lett.*, **36**, L1780, doi:10.1029/2009GL039 968.

Žagar, N., E. Andersson, and M. Fisher, 2005: Balanced tropical data assimilation based on a study of equatorial waves in ECMWF short-range forecast errors. *Quart. J. Roy. Meteorol. Soc.*, **131**, 987–1011.

Wickert, J., et al., 2001: Atmosphere sounding by GPS radio occultation: First results from CHAMP. *Geophys. Res. Lett.*, **28**, 3263–3266.

Wickert, J., et al., 2009: GPS radio occultation: results from CHAMP, GRACE and FORMOSAT-3/COSMIC. *Terrestrial Atmospheric and Oceanic Sciences*, **20**, 35–50.